International Journal of Engineering

Journal Homepage: www.ije.ir

Determination of Fiber Direction in High Angular Resolution Diffusion Images using Spherical Harmonics Functions and Wiener Filter

M. Hashemi Kamangar[a*], M. R. Karami Mollaeia[a], R. Ghaderi[b]

[a] *Faculty of Electrical and Computer Engineering, Babol University of Technology, Babol, Iran*
[b] *Faculty of Control Engineering, Shahid Beheshti University, Tehran, Iran*

PAPER INFO

Paper history:
Received 12 May 2015
Received in revised form 28 February 2016
Accepted 03 March 2016

Keywords:
Diffusion Tensor MRI
High Angular Resolution Diffusion Imaging
Spherical Deconvolution
Wiener Filter
Orientation Distribution Function

ABSTRACT

Diffusion tensor imaging (DTI) MRI is a noninvasive imaging method of the cerebral tissues whose fibers directions are not evaluated correctly in the regions of the crossing fibers. For the same reason, the high angular resolution diffusion images (HARDI) are used for estimation of the fiber direction in each voxel. One of the main methods to specify the direction of fibers is usage of the spherical deconvolution. The spherical deconvolution is a method which is very sensitive to noise and creates negative values in the orientation distribution function (ODF) of the fiber. To solve this problem, methods such as Laplace-Beltrami regularized spherical deconvolution (LB-SD), the gradient based spherical deconvolution (GB-SD) and the constrained spherical deconvolution (CSD) are used. In this paper, the method for SD based on Wiener filter (WB-SD) is presented. Regarding the results, the direction of the crossing fibers is specified correctly. The proposed algorithm has specified the direction of the fibers as zero degree with 4.9 standard deviation and 89.9 degree with 3.6 standard deviation against two crossing fibers with 90 degree angle.

doi: *10.5829/idosi.ije.2016.29.03c.07*

1. INTRODUCTION

Demyelination causes loss of nerve fibers and therefore message could not be transmitted through the fiber and it causes diseases such as, multiple sclerosis, Alzheimer's and krabbe [1-3]. These diseases, for example Alzheimer's, is a progressive neurodegenerative disorder that impairs memory, cognitive function, thinking, behavior and language [4].

The diffusion tensor imaging (DTI) MRI is a noninvasive imaging method of the cerebral tissues in which the brain is imaged by exerting the gradient vector in different directions and it is useful for detection of demyelination in the brain [5]. In each taken image, in the fibers which are exerted in the same direction with the gradient vector, the signals are weakened faster and appear darker in the image and these images can be used for direction finding of the cerebral fibers. The Stejskal-Tanner imaging sequences are used to measure the spread of water molecules [6]. The usual form of Stejskal-Tanner formula under the Gaussian assumptions is as follows:

$$S = S_0 e^{-bg^T \mathbf{D} g} \quad (1)$$

where b is the attenuation coefficient, S_0 diffusion signal without diffusion gradient (b=0), D diffusion tensor, and g the imaging gradient direction.

Due to the tensor model's limitation in specifying the crossing and kissing fibers in each voxel [7], the high angular resolution diffusion imaging (HARDI) is used which take images of brain in 60 different gradient directions at least. While DTI method needs 6 gradient directions to specify diffusion tensor [8, 9], the higher angular resolution creates an exacter 3D pattern of water penetration inside the voxel [7]. Q-ball imaging is used to determine ODF of penetration [10]. Q-ball imaging (QBI) approximates ODF of penetration directly from HARDI raw measurements on the unit circle using Funk-Radon transform [11, 12]. ODF of penetration that calculated by QBI is the blurred form of fiber

*Corresponding Author's Email: Me.hashemi@stu.nit.ac.ir (M. Hashemi Kamangar)

Please cite this article as: M. Hashemi Kamangar , M.R. Karami Mollaeia, R. Ghaderi, Determination of Fiber Direction in High Angular Resolution Diffusion Images (HARDI) Using Spherical Harmonics Functions and Wiener Filter, International Journal of Engineering (IJE), TRANSACTIONS C: Aspects Vol. 29, No. 03, (March 2016) 328-336

distribution [13]. To solve the blurring problem in QBI, spherical deconvolution is used. It assumes HARDI signal as spherical convolution of fiber response function and fiber function [13, 14]. The fiber direction is determined by spherical deconvolution. Due to the presence of noise in HARDI signal, spurious peaks and negative values appear in spherical deconvolution method. To solve this problem, methods such as FSD which uses low pass filter [15], GB-SD and LB-SD that use minimization of least square error with a square gradient constraint and square of Laplace-Beltrami operator [8, 16] and constraint spherical deconvolution method which uses repetitive method with imposing nonnegative constraint on ODF of renovated fiber [17, 18] are presented.

In nonnegative Spherical Deconvolution (NNSD), non-negativity is achieved by representing the square root of the ODF as a linear combination of SH basis functions [19, 20].

In this paper, ODF of fiber is calculated by combining spherical deconvolution and Wiener filter without using repetitive methods and matrix operation, and only by simple division in calculating spherical harmonic expansion coefficients.

2. METHODS

Spherical harmonics is appropriate mathematical tool to represent spherical data [21, 22]. Spherical harmonics transform is the equivalent of Fourier transform in the 3D space. Since HARDI images are spherical, spherical harmonics series is used for expansion of HARDI images [23].

2. 1. Spherical Harmonic Functions Each signal in spherical coordinates is written as the linear combination of spherical functions

$$S(\theta,\varphi)=\sum_{l=0}^{\infty}\sum_{m=-l}^{l}c_l^m Y_l^m(\theta,\varphi) \quad (2)$$

in which c_l^m is coefficients of expansion and $Y_l^m(\theta,\varphi)$ the spherical harmonic function of order l and degree m is as follows:

$$Y_l^m=\sqrt{\frac{2l+1}{4\pi}\frac{(l-m)!}{(l+m)!}}P_l^m(cos\theta)e^{im\varphi} \quad (3)$$

$P_l^m(.)$ is the Legendre function of order l and degree m [24]. Since the diffusion images are real, the modified spherical harmonics, which are real as well, are used to expand the diffusion signals [8].

$$Y_{lm}=\begin{cases}\sqrt{2}(-1)^m Im(Y_l^{|m|}) & m<0\\ Y_l^m & m=0\\ \sqrt{2}\,(-1)^m Re(Y_l^m) & m>0\end{cases} \quad (4)$$

Also regarding the antipodal symmetric property of the diffusion images, and since only the harmonic functions with even order have the antipodal symmetric property, therefore, the spherical harmonics with even order are used to expand signals:

$$S(\theta,\varphi)=\sum_{l=0,2,4,\ldots}\sum_{m=-l}^{l}s(l,m)Y_{lm}(\theta,\varphi) \quad (5)$$

The ODF of diffusion images are computed by projection of signal on the unit sphere in different directions by usage of Funk-Radon transform (FRT).

To calculate FRT, the diffusion signal ($S(\boldsymbol{w})$) is replaced by spherical harmonics series, and FRT can be calculated in terms of spherical harmonics coefficients.

$$\begin{aligned}ODF(\boldsymbol{u})&=\mathcal{G}\left[S/_{S_0}\right](\boldsymbol{u})=\\ &\frac{1}{S_0}\int_{|w|=1}\delta(\boldsymbol{u}^T\boldsymbol{w})S(\boldsymbol{w})d\boldsymbol{w}=\\ &\sum_{l=0,2,4,\ldots}\sum_{m=-l}^{l}\frac{2\pi P_l(0)}{S_0}s(l,m)Y_{lm}(\boldsymbol{u})\end{aligned} \quad (6)$$

S_0 is signal without diffusion (b=0) and $P_l(0)$ is Legendre function with order *l* evaluated at zero.

2. 2. Spherical Deconvolution In diffusion images, the signal received in each voxel can be assumed as the convolution of symmetric response function and impulse function [15,17]. The impulse functions specify the direction of fibers in that voxel. In Figure 1, R(θ) is the symmetric impulse response function and F(θ,φ) is direction of fibers and diffusion signals which are shown as convolution R(θ) and F(θ,φ).

If response function, diffusion signal, and spherical impulse function have respectively the spherical harmonic coefficients r(l,m), s(l,m) and δ(l,m), the fiber direction is computed using the following equations [8, 15, 17] :

$$\delta(l,m)=Y_{l,0} \quad (7)$$

$$f(l,m)=s(l,m)/R(l,m) \quad (8)$$

$$R(l,m)=\frac{r(l,0)}{\delta(l,m)} \quad (9)$$

2. 3. Retrieval of Fiber Direction For Noise Signal In common MRI system, data are considered as the real and imaginary sections of a complex value. The amplitude of this value is used as the MRI signal. Noise of the real and imaginary sections has the Gaussian distribution and thus MRI signal noise is modeled as Rician noise [25, 26].

Noise creates spurious peaks and negative values on the unit sphere which cause making unreal directions. To reduce the noise effect, the filtered spherical deconvolution (fSD) is used. Spherical harmonic coefficients *s(l,m)* in the Equation (8) of order l are multiplied in a number less than or equal to 1. As the order *l* increases, the number gets smaller. For example orders 0, 2 and 4 are multiplied by 1, and orders 6 and 8 multiplied by 0.8 and 0.1, respectively [15, 17].

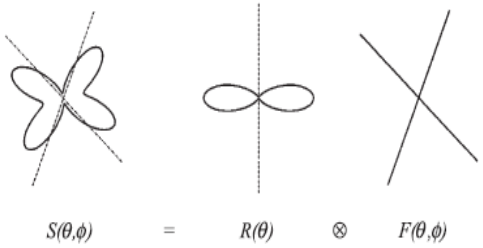

Figure 1. Diffusion signal as convolution of impulse response function and impulse functions [15]

In the method of gradient based spherical deconvolution (GB-SD), a constrained function is defined as square of gradient norm fiber ODF and in the method of Laplace-Beltrami regularized spherical deconvolution is defined as square of Laplace-Beltrami operator of fiber ODF in all directions on the unit sphere. By minimizing the function, the fiber direction is specified [8, 16] and fiber direction of HARDI raw signal is computed as the following equation:

$$F = ((BR)^T BR + \lambda L)^{-1}(BR)^T S \quad (10)$$

R is rotational harmonic decomposition of the response function with the diagonal array specified at Equation (9), S is HARDI signal, λ regularization parameter, L diagonal matrix with the values of $l(l+1)$ for GB-SD method and $l^2(l+1)^2$for LB-SD method and F fiber direction. B is the matrix of spherical harmonic basis functions with dimensions K (equal to number of gradient direction) and $L = (L_{max}+1)(L_{max}+2)/2$ (equal to number of spherical harmonic coefficients) is as follows:

$$B = \begin{bmatrix} Y_{0,0}(\theta_1,\varphi_1) & Y_{2,-2}(\theta_1,\varphi_1) & \cdots & Y_{L,L}(\theta_1,\varphi_1) \\ Y_{0,0}(\theta_2,\varphi_2) & Y_{2,-2}(\theta_2,\varphi_2) & \cdots & Y_{L,L}(\theta_2,\varphi_2) \\ \vdots & & \ddots & \vdots \\ Y_{0,0}(\theta_K,\varphi_K) & Y_{2,-2}(\theta_K,\varphi_K) & \cdots & Y_{L,L}(\theta_K,\varphi_K) \end{bmatrix} \quad (11)$$

2. 4. Proposed Method (Wiener Based Spherical Deconvolution (Wb-Sd)) Two signals convolution in spherical coordinates have the spherical harmonic expansion as the Equation (12) [22].

$$S(\theta,\varphi) = F(\theta,\varphi) * H(\theta,\varphi) \overset{SHT}{\longleftrightarrow} s(l,m) = 2\pi\sqrt{\frac{4\pi}{2l+1}}h(l,0)f(l,m) \quad (12)$$

where $f(l,m)$, $h(l,m)$ and $s(l,m)$ are respectively the spherical harmonic expansion coefficients of signals $F(\theta,\varphi)$ (fibers direction) and $H(\theta,\varphi)$ (response function) and the diffusion signal. Since in spherical harmonic expansion, the truncated series is used, the response function $H(\theta,\varphi)$ is defined in z axis direction in order to minimize truncation error.

The response function is generated by using Equation (1) and D diffusion tensor in the direction of z axis with $D_{xx}=D_{yy}=0$ and $D_{zz}=\lambda$, and also g is gradient vector in different directions. The spherical harmonic expansion of fiber can be computed as follows:

$$f(l,m) = \frac{1}{2\pi\sqrt{\frac{4\pi}{2l+1}}h(l,0)}s(l,m) \quad (13)$$

Since diffusion signal is noisy, the direction usage of above formula causes a lot of negative values in the fiber ODF [27]. In the proposed method, the Wiener filter is used to retrieve the fiber direction which causes reduction of number of negative values in fiber ODF. In case of existence of noise, this filter is used to improve the performance of the inverse system in the frequency field [28].

$$G(f) = \frac{1}{H(f)}\frac{|H(f)|^2}{|H(f)|^2+A} \quad (14)$$

H(f) is system transform function, G(f) inverse system transform function and A constant number. The definition of Wiener filter in spherical deconvolution is used to retrieve fiber direction in HARDI images (see appendix A1).

$$f(l,m) = \frac{1}{r(l,m)}\frac{|r(l,m)|^2}{|r(l,m)|^2+A}\,s(l,m) \quad (15)$$

where $r(l,m) = 2\pi\sqrt{\frac{4\pi}{2l+1}}h(l,0)$, A is constant value and |.| the amplitude operator.

3. DATA

The synthetic data of HARDI signal in one voxel is created by using multi-tensor model [29] $S(g) = S_0\sum p_j e^{-bg^T Dg}$ with b=3000s/mm^2, λ_1=0.0015, $\lambda_2=\lambda_3$=0.0003 and S_0=100 in 64 gradient directions with 2 crossing fibers of angle 75, 90, θ=60 and p_j is volume fraction of jth fiber ($p_1=p_2$=0.5). The Rician noise with signal to noise ratio $\left(SNR = \frac{S_0}{\sigma}\right) SNR = 5, 10, 15, 20$ is added to signal S.

The general phantom data [30] with b=1500 s/mm^2 and spatial resolution 3mm are being used.

4. RESULTS

The methods SD, fSD, LB-SD with constant λ equal to 5×10^{-5} ،GD-SD, GD-SD with constant λ equal to 5×10^{-3} and Wiener-SD have been carried out on the synthetic data 100 times. Since LB-SD and GD-SD methods are sensitive to the value of λ, this value should be correctly selected. In this article the reference values [8] are used. In Wiener-SD method, the value of A is determined from the following equation:

$$A = 0.01 \times \langle |r(l,m)|^2 \rangle \quad (16)$$

<.> is average operator. In Figures 2, 3 and 4 fiber orientation distribution (FOD) are shown respectively for angles 60 degrees, 75 degrees and 90 degrees and results of 100 noise trials have been extracted.

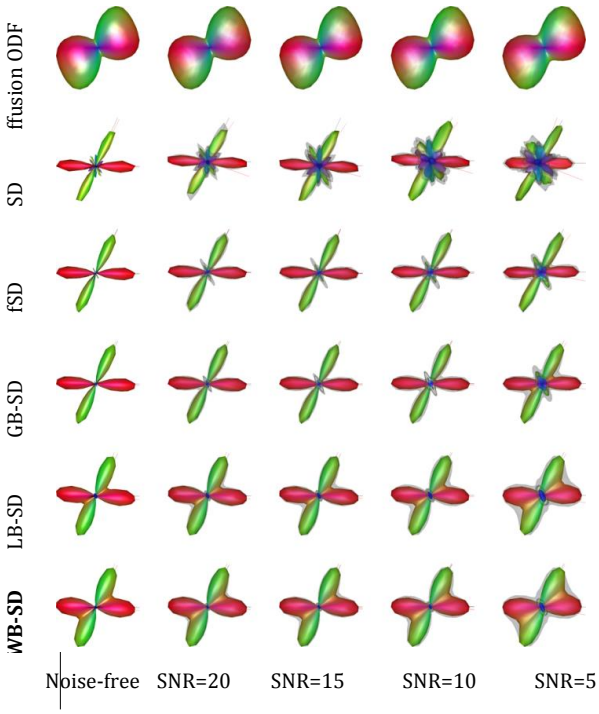

Figure 2. FOD for data with 2 crossing fibers in directions 0 and 60 degrees against xy plane. Opaque surfaces corresponding to average FOD with 100 noise trials and transparent surfaces corresponding average FOD are plus twice as much of standard deviation.

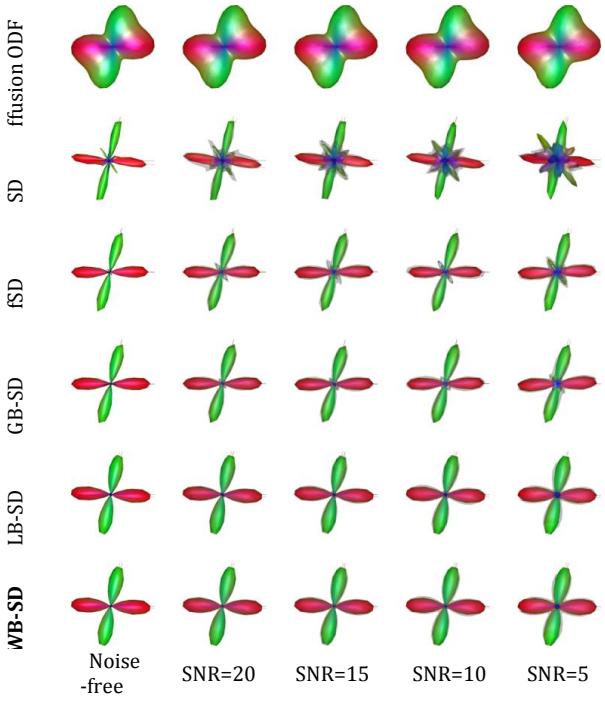

Figure 3. FOD for data with 2 crossing fibers in directions 0 and 75 degrees against xy plane. Opaque surfaces corresponding to average FOD with 100 noise trials and transparent surfaces corresponding average FOD are plus twice as much of standard deviation

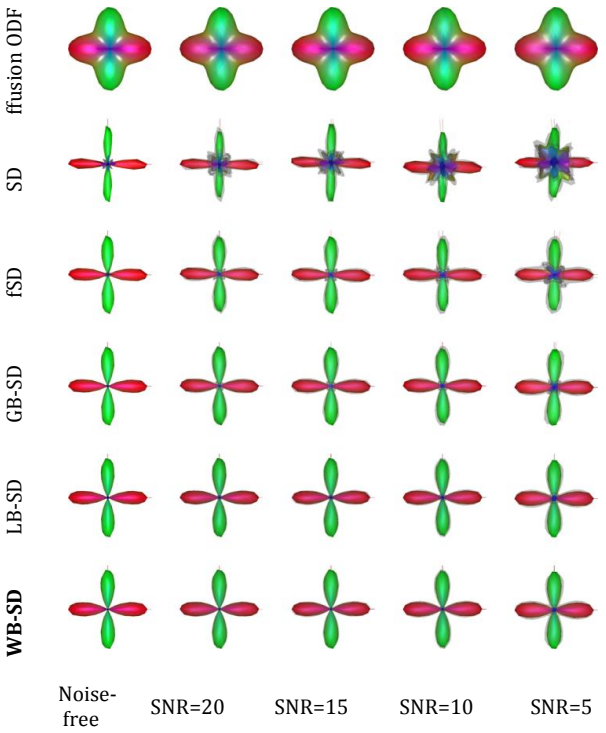

Figure 4. FOD for data with 2 crossing fibers in directions 0 and 90 degrees against xy plane. Opaque surfaces corresponding to average FOD with 100 noise trials and transparent surfaces corresponding to average FOD are plus twice as much of standard deviation.

The opaque and transparent surfaces corresponding to the average FOD are plus twice as much of standard deviation. The red lines are ground true??? fiber directions and blue lines are computed directions (maximum value in ODF).

In all methods to eliminate negative values in orientation distribution function, the negative values of obtained ODF are equaled to zero. As seen from the results, in SD and FSD methods with reduction of signal to noise ratio, spurious peaks are increased but in WB-SD method without using any regularization parameter, spurious peaks are eliminated, while GB-SD and LB-SD methods use regularization parameter.

In Figures 5, 6 and 7, fiber average computed direction and its standard deviation against 100 trials, for synthetic data with 2 crossing fibers with zero and 60, 75 and 90 degree, respectively with respective to xy plane are shown. θ is the angle with x axis and φ the angle with xy plane in the spherical coordinates.

According to Figures 5 - 7, it is observed that there are not any significant differences between the calculated directions of WB-SD method and GB-SD, LB-SD methods. It is seen that with increasing the angle between crossing fibers, the accuracy of the calculation increases and at low signal-to-noise ratio (SNR=5), calculation of standard deviation increases in each of the

three methods and at low signal-to-noise ratio (SNR=5), standard deviation is minimum in WB-SD method.

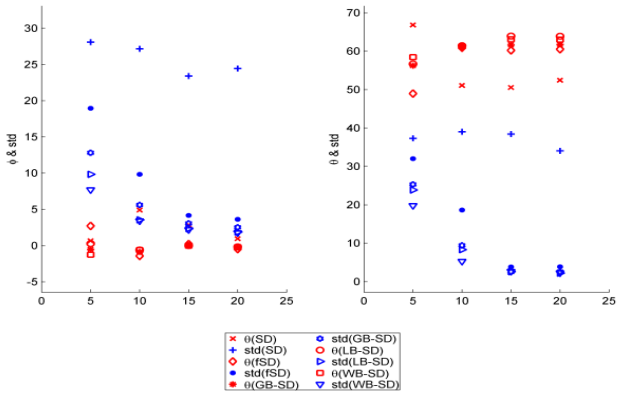

Figure 5. The fiber computed direction and its standard deviation for the fiber with true angles θ=60 (right figure) and φ=0 (left figure) in synthetic data with two 60 degrees crossing fibers (θ is the angle with x axis and φ angle with xy plane).

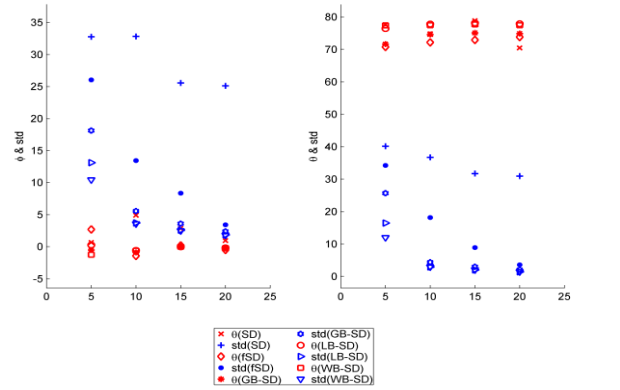

Figure 6. The fiber computed direction and its standard deviation for the fiber with true angles θ=75 (right figure) and φ=0 (left figure) in synthetic data with two 75 degrees crossing fibers (θ is the angle with x axis and φ is angle with xy plane).

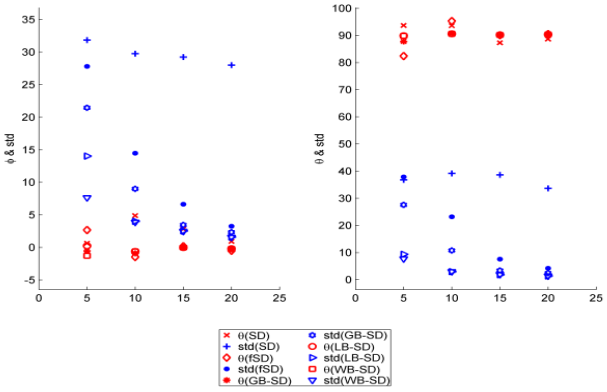

Figure 7. The fiber computed direction and its standard deviation for the fiber with true angles θ=90 (right figure) and φ=0 (left figure) in synthetic data with two 90 degrees crossing fibers (θ is the angle with x axis and φ is angle with xy plane).

In Table 1, fiber average computed direction and its standard deviation against 100 trials for synthetic data with 2 crossing fibers with zero and 75 degree angles with respective to xy plane are shown (corresponding to Figure 6). θ is the angle with x axis and φ the angle with xy plane in the spherical coordinates.

In Figure 8 the result of algorithm WB-SD on the phantom presented in 2009 MICCAI conference is shown. In the left side figure the fiber ODF for HARDI signal and in the right side figure the fiber ODF with WB-SD method is shown. Also, Figure 9 indicates the result of proposed algorithm on the region of interest (crossing fibers region) which in left and right figures, the main fiber ODF and ODF with WB-SD are shown respectively. As seen in Figure 9, the orientations of crossed fibers are determined correctly.

TABLE 1. The fiber computed direction and its standard deviation for the fiber with true angles θ=75 and φ=0 in synthetic data with two 75 degrees crossing fibers (θ is the angle with x axis and φ is angle with xy plane).

3	SNR=20				SNR=15				SNR=10				SNR=5			
	φ	std(φ)	θ	std(θ)	φ	std(φ)	θ	std(θ)	φ	std(φ)	θ	std(θ)	φ	std(φ)	θ	std(θ)
SD	-1.2	25.2	70.5	31	2.4	25.6	78.9	31.8	-0.2	32.9	74.9	36.8	-2	32.8	77.7	40.2
fSD	-0.4	3.4	73.8	3.6	-0.3	8.4	72.9	8.9	-1.1	13.5	72.2	18.2	-1.4	26.1	70.8	34.3
GB-SD	-0.2	2.4	74.9	2.1	-0.2	3.6	75.1	3	-0.9	5.6	74.6	4.4	-1.8	18.2	71.7	25.7
LB-SD	-0.2	1.9	78	1.5	-0.2	2.6	78.2	2.1	-0.4	3.8	77.9	3	1.1	13.2	76.4	16.5
WB-SD	-0.2	1.8	77.5	1.5	-0.2	2.5	77.7	2.1	-0.3	3.6	77.5	3	-0.2	10.5	77.4	12

Figure 8. The result of algorithm on the phantom presented in MICCAI 2009 fiber Cup [30] . Left side shows main fiber ODF and Right side shows fiber ODF with WB-SD method.

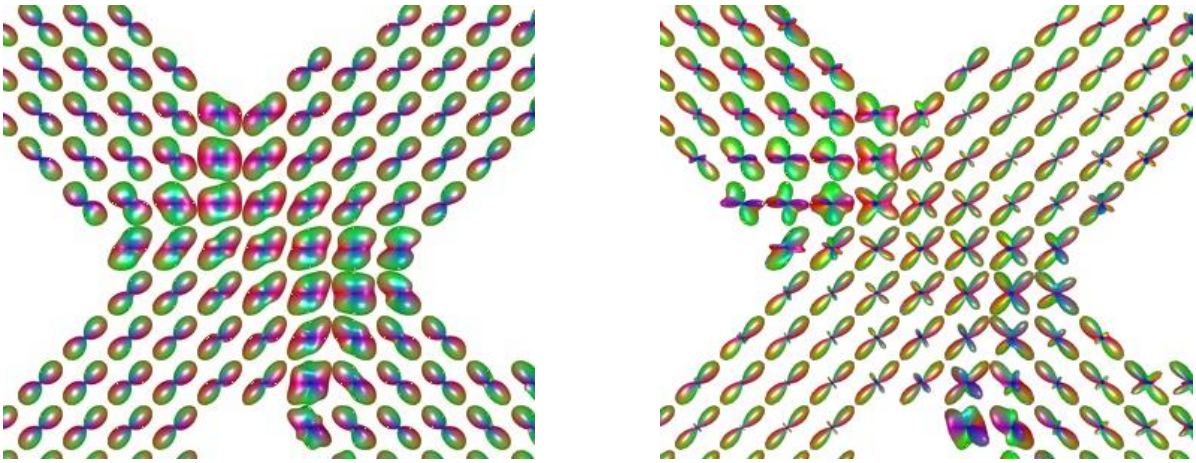

Figure 9. The result of algorithm on the phantom crossing fibers presented in MICCAI 2009 fiber Cup [30]. Left side shows main fiber ODF and Right side shows fiber ODF with WB-SD method

5. CONCLUSION

In this article, the proposed method of WB-SD was compared with the methods SD, fSD, LB-SD and GB-SD. In all methods, the omission of noise to improve the SNR has not been done and noisy values of signal are used to compute ODF. Also, in all methods for eliminating negative values in orientation distribution function, the negative values obtained for ODF are equaled to zero. In the proposed method, the Wiener filter was used in spherical deconvolution and every spherical harmonic expansion coefficient has been computed independently (Equation (15)). As the results show, in SD and FSD methods spurious peaks are increased with signal to noise reduction, but in WB-SD method without using any regularization parameter they are omitted while in GB-SD and LB-SD methods regularization parameter is used. The results indicate that the proposed method correctly evaluates the fiber angles against the different values of signal to noise.

The results of algorithm upon the phantom data show that the WB-SD method recognizes the fiber crossing direction correctly which the angles are modeled as two fibers. Moreover, it recognizes correctly the direction in the ellipsoid regions which are modeled as one fiber.

6. REFRENCES

1. Hesseltine, S. M., Ge, Y. and Law, M., "Applications of diffusion tensor imaging and fiber tractography". ***Applied Radiology***.Vol. 36, NO. 5, (2007), 8.
2. Pandit, L., "Differential diagnosis of white matter diseases in the tropics: An overview". ***Annals of Indian Academy of Neurology***.Vol. 12, NO. 1, (2009), 12-21.

3. Escolar, M. L., Poe, M. D., Smith, J. K., Gilmore, J. H., Kurtzberg, J., Lin, W. and Styner, M., "Diffusion tensor imaging detects abnormalities in the corticospinal tracts of neonates with infantile Krabbe disease". ***American Journal of Neuroradiology***.Vol. 30, NO. 5, (2009), 1017-1021.
4. Dehghan, H., Pouyan, A. and Hassanpour, H., "Detection of alzheimer's disease using multitracer positron emission tomography imaging". ***International Journal of Engineering-Transactions A: Basics***.Vol. 27, NO. 1, (2013), 51-56.
5. Daoudi, Y., Ameri, L. and Dadpour, B., "The role of diffusion-weighted MRI on the study of brain complications related to heroin abuse". ***Reviews in Clinical Medicine***.Vol. 2, NO. 3, (2015), 144-146.
6. Stejskal, E. and Tanner, J., "Spin diffusion measurements: spin echoes in the presence of a time-dependent field gradient". ***The Journal of Chemical Physics***.Vol. 42, NO. 1, (1965), 288-292.
7. Berman, J. I., Lanza, M. R., Blaskey, L., Edgar, J. C. and Roberts, T. P., "High angular resolution diffusion imaging probabilistic tractography of the auditory radiation". ***American Journal of Neuroradiology***.Vol. 34, NO. 8, (2013), 1573-1578.
8. Descoteaux, M., High angular resolution diffusion MRI: from local estimation to segmentation and tractography, in, Editor^Editors. (2010), INRIA Sophia Antipolis, France.
9. Özarslan, E., Shepherd, T. M., Vemuri, B. C., Blackband, S. J. and Mareci, T. H., "Resolution of complex tissue microarchitecture using the diffusion orientation transform (DOT)". ***NeuroImage***.Vol. 31, NO. 3, (2006), 1086-1103.
10. Tuch, D. S., "Q-ball imaging". ***Magnetic Resonance in Medicine***.Vol. 52, NO. 6, (2004), 1358-1372.
11. Descoteaux, M., Angelino, E., Fitzgibbons, S. and Deriche, R., "Regularized, fast, and robust analytical Q-ball imaging". ***Magnetic Resonance in Medicine***.Vol. 58, NO. 3, (2007), 497-510.
12. Acqua, F. D., Rizzo, G., Scifo, P., Clarke, R. A., Scotti, G. and Fazio, F., "A model-based deconvolution approach to solve fiber crossing in diffusion-weighted MR imaging". ***Biomedical Engineering, IEEE Transactions on***.Vol. 54, NO. 3, (2007), 462-472.
13. Aganj, I., Lenglet, C., Sapiro, G., Yacoub, E., Ugurbil, K. and Harel, N., "Reconstruction of the orientation distribution function in single-and multiple-shell q-ball imaging within constant solid angle". ***Magnetic Resonance in Medicine***.Vol. 64, NO. 2, (2010), 554-566.
14. Jian, B. and Vemuri, B. C., "A unified computational framework for deconvolution to reconstruct multiple fibers from diffusion weighted MRI". ***Medical Imaging, IEEE Transactions on***. Vol. 26, No. 11, (2007), 1464-1471.
15. Tournier, J.-D., Calamante, F., Gadian, D. G. and Connelly, A., "Direct estimation of the fiber orientation density function from diffusion-weighted MRI data using spherical deconvolution". ***NeuroImage***.Vol. 23, NO. 3, (2004), 1176-1185.
16. Sakaie, K. E. and Lowe, M. J., "An objective method for regularization of fiber orientation distributions derived from diffusion-weighted MRI". ***NeuroImage***.Vol. 34, NO. 1, (2007), 169-176.
17. Tournier, J.-D., Calamante, F. and Connelly, A., "Robust determination of the fibre orientation distribution in diffusion MRI: non-negativity constrained super-resolved spherical deconvolution". ***NeuroImage***.Vol. 35, NO. 4, (2007), 1459-1472.
18. Tournier, J.-D., Yeh, C.-H., Calamante, F., Cho, K.-H., Connelly, A. and Lin, C.-P., "Resolving crossing fibres using constrained spherical deconvolution: validation using diffusion-weighted imaging phantom data". ***Neuroimage***.Vol. 42, NO. 2, (2008), 617-625.
19. Cheng, J., Deriche, R., Jiang, T., Shena, D. and Yap, P.-T., "Non-Negative Spherical Deconvolution (NNSD) for estimation of fiber Orientation Distribution Function in single-/multi-shell diffusion MRI". ***NeuroImage***.Vol. 101, (2014), 750-764.
20. Cheng, J., Jiang, T. and Deriche, R., "Nonnegative definite EAP and ODF estimation via a unified multi-shell HARDI reconstruction," in Medical Image Computing and Computer-Assisted Intervention–MICCAI 2012, ed: Springer, (2012), 313-321.
21. Dokmanic, I. and Lu, Y. M., "Sampling Sparse Signals on the Sphere: Algorithms and Applications". ***Signal Processing, IEEE Transactions on***.Vol. 64, NO. 1, (2016), 189-202.
22. Driscoll, J. R. and Healy, D. M., "Computing Fourier transforms and convolutions on the 2-sphere". ***Advances in Applied Mathematics.*** Vol. 15, NO. 2, (1994), 202-250.
23. Frank, R. L., "Characterization of anisotropy in high angular resolution diffusion-weighted MRI". ***Magnetic Resonance in Medicine***.Vol. 47, NO. 6, (2002), 1083-1099.
24. Arfken, G. B. and Weber, H. J., Mathematical Methods for Physicists: ***Academic Press,*** (2005).
25. Canales-Rodriguez, E., J., Daducci, A., Sotiropoulos, S., N., Caruyer, E., Aja-Fernandez, S., Radua, J., Mendizabal, Y., Yosu, Iturria-Medina, Y., Melie-Garcia, L., Aleman-Gomez, Y. and Thiran, J.-P., "Spherical deconvolution of multichannel diffusion MRI data with non-Gaussian noise models and total variation spatial regularization" ***NeuroImage***. Vol. 25, (2000), 1259–1272.
26. V., H. and Borna, K., "An Adaptive Hierarchical Method Based on Wavelet and Adaptive Filtering for MRI Denoising". ***International Journal of Engineering-TRANSACTIONS A: Basics*** Vol. 29, NO. 1, (2016), 31-39.
27. Tournier, J. D., Calamante, F. and Connelly, A., "Robust determination of the fibre orientation distribution in diffusion MRI: Non-negativity constrained superresolved spherical deconvolution". ***NeuroImage***.Vol. 35, (2007), 1459–1472.
28. Nadernejad, E., Hassanpour, H. and Miar, H., "Image restoration using a PDE-based approach". ***International Journal of Engineering-TRANSACTIONS B: Applications***. Vol. 20, NO. 3, (2007).
29. Schultz, T., Westin, C.-F. and Kindlmann, G., "Multi-diffusion-tensor fitting via spherical deconvolution: a unifying framework," in ***Medical Image Computing and Computer-Assisted Intervention–MICCAI***, ed: Springer, (2010), 674-681.
30. Fillard, P., Descoteaux, M., Goh, A., Gouttard, S., Jeurissen, B., Malcolm, J., Ramirez-Manzanares, A., Reisert, M., Sakaie, K. and Tensaouti, F., "Quantitative evaluation of 10 tractography algorithms on a realistic diffusion MR phantom". ***Neuroimage***.Vol. 56, No. 1, (2011), 220-234.

APPENDIX

Two signals convolution in the spherical coordinates with added noise has the spherical harmonic expansion as in the Equation E1 .The noise is independent of the signal.

$$S(\theta,\varphi) = H(\theta,\varphi) * F(\theta,\varphi) + N(\theta,\varphi) \quad \text{E1}$$

$$S(\theta,\varphi) = \sum_l \sum_m s(l,m) Y_l^m(\theta,\varphi) \quad \text{E2}$$

$$s(l,m) = 2\pi \sqrt{\frac{4\pi}{2l+1}} h(l,0) f(l,m) + n(l,m) \quad \text{E3}$$

where, $f(l, m)$, $h(l, m)$, $s(l, m)$ and $n(l,m)$ are the spherical harmonic expansion coefficients of the signals

$F(\theta,\varphi)$ (fibers orientations) and $H(\theta,\varphi)$ (response function), diffusion signal and noise respectively.

We can recover the spherical harmonic coefficients of the diffusion signal with usage of deconvolution as below:

$$\hat{f}(l,m) = 2\pi\sqrt{\frac{4\pi}{2l+1}}k(l,0)s(l,m) \quad \text{E4}$$

$$\hat{F}(\theta,\varphi) = \sum_l \sum_m \hat{f}(l,m) Y_l^m(\theta,\varphi) \quad \text{E5}$$

$\hat{F}(\theta,\varphi)$ can be calculated with usage of least square optimization problem as

$$\begin{aligned} e = E\left\{\left\|\left(F(\theta,\varphi)-\hat{F}(\theta,\varphi)\right)\right\|^2\right\} = E\left\{\left(F(\theta,\varphi)-\right.\right. \\ \left.\left.\hat{F}(\theta,\varphi)\right)\overline{\left(F(\theta,\varphi)-\hat{F}(\theta,\varphi)\right)}\right\} = \\ E\{F(\theta,\varphi)\overline{F(\theta,\varphi)}\} - E\{F(\theta,\varphi)\overline{\hat{F}(\theta,\varphi)}\} - \\ E\{\hat{F}(\theta,\varphi)\overline{F(\theta,\varphi)}\} + E\{\hat{F}(\theta,\varphi)\overline{\hat{F}(\theta,\varphi)}\} \end{aligned} \quad \text{E6}$$

Each term of right hand side of equation is expanded with use of spherical harmonics function

$$\begin{aligned} E\{F(\theta,\varphi)\overline{F(\theta,\varphi)}\} = \\ E\left\{\sum_l \sum_m f(l,m) Y_l^m(\theta,\varphi) \sum_{l'} \sum_{m'} \bar{f}(l',m') \bar{Y}_{l'}^{m'}(\theta,\varphi)\right\} = \\ \sum_l \sum_m \sum_{l'} \sum_{m'} f(l,m)\bar{f}(l',m') E\{Y_l^m(\theta,\varphi)\bar{Y}_{l'}^{m'}(\theta,\varphi)\} = \\ \sum_l \sum_m \sum_{l'} \sum_{m'} f(l,m)\bar{f}(l',m')\delta_{ll'}\delta_{mm'} = \\ \sum_l \sum_m f(l,m)\bar{f}(l,m) = \sum_l (2l+1) S_{FF}(l) \end{aligned} \quad \text{E7}$$

$S_{FF}(l)$ is angular power spectrum that is equal $\frac{1}{(2l+1)}\sum_m f(l,m)\bar{f}(l,m)$.

The second term of Equation E6, can be written as spherical harmonics function such as Equation E7.

Due to the uncorrelated signal and noise, the cross power spectrum between noise and signal ($S_{FN}(l)$) is zero

$$\begin{aligned} E\left\{F(\theta,\varphi)\overline{\hat{F}(\theta,\varphi)}\right\} = \sum_l \sum_m f(l,m)\bar{\hat{f}}(l,m) = \\ \sum_l \sum_m f(l,m) 2\pi\sqrt{\frac{4\pi}{2l+1}}\overline{k(l,0)s(l,m)} = \\ \sum_l \left((2\pi)^2 \frac{4\pi}{2l+1} \overline{h(l,0)}\ \overline{k(l,0)}\ (2l+1) S_{FF}(l) + \right. \\ 2\pi\sqrt{\frac{4\pi}{2l+1}}\overline{k(l,0)}\ (2l+ \\ \left. 1) S_{FN}(l)\right) = \sum_l (2\pi)^2 \frac{4\pi}{2l+1} \overline{h(l,0)}\ \overline{k(l,0)}\ (2l+ \\ 1) S_{FF}(l) \end{aligned} \quad \text{E8}$$

Similarly, the third term of Equation E6 can be written based on angular power spectrum of fiber.

$$\begin{aligned} E\{\hat{F}(\theta,\varphi)\overline{F(\theta,\varphi)}\} = \sum_l \sum_m \hat{f}(l,m)\overline{f(l,m)} = \\ \sum_l \sum_m 2\pi\sqrt{\frac{4\pi}{2l+1}} k(l,0) s(l,m)\overline{f(l,m)} = \\ \sum_l (2\pi)^2 \frac{4\pi}{2l+1} h(l,0)\ k(l,0)\ (2l+1) S_{FF}(l) \end{aligned} \quad \text{E9}$$

Due to the cross power spectrum between noise and signal is zero, $E\left\{\hat{F}(\theta,\varphi)\overline{\hat{F}(\theta,\varphi)}\right\}$ can be written in terms of $S_{FF}(l)$ and $S_{NN}(l)$

$$\begin{aligned} E\left\{\hat{F}(\theta,\varphi)\overline{\hat{F}(\theta,\varphi)}\right\} = \sum_l \sum_m \hat{f}(l,m)\bar{\hat{f}}(l,m) = \\ \sum_l (2\pi)^2 \frac{4\pi}{2l+1}\left((2\pi)^2 \frac{4\pi}{2l+1} k(l,0)\overline{k(l,0)} h(l,0)\ \overline{h(l,0)}\right. \\ \left. (2l+1) S_{FF}(l) + k(l,0)\overline{k(l,0)}\ (2l+1) S_{NN}(l)\right) \end{aligned} \quad \text{E10}$$

To find the minimum error, we calculate the derivative with respect to $k(l,0)$ and set it equal to zero.

$$\begin{aligned} \frac{\partial e}{\partial k(l,0)} = (2\pi)^2 \frac{4\pi}{2l+1}\left(-h(l,0)\ k(l,0)\ (2l+\right. \\ 1) S_F(l) + \\ (2\pi)^2 \frac{4\pi}{2l+1} k(l,0)\overline{k(l,0)} h(l,0)\overline{h(l,0)}(2l+ \\ \left. 1) S_F(l) + k(l,0)\overline{k(l,0)}\ (2l+1) S_N(l)\right) = 0 \end{aligned} \quad \text{E11}$$

By solving Equation E11, $\overline{k(l,0)}$ can be determined

$$\overline{k(l,0)} = \frac{h(l,0)\ S_{FF}(l)}{(2\pi)^2 \frac{4\pi}{2l+1} h(l,0)\overline{h(l,0)} S_{FF}(l) + S_{NN}(l)} \quad \text{E12}$$

By some calculations, $k(l,0)$ can be written in terms of $h(l,0)$, $S_{NN}(l)$ and $S_{FF}(l)$.

$$\begin{aligned} k(l,0) = \frac{\overline{h(l,0)}}{\left\|2\pi\sqrt{\frac{4\pi}{2l+1}}h(l,0)\right\|^2 + S_{NN}(l)/S_{FF}(l)} = \\ \frac{1}{(2\pi)^2 \frac{4\pi}{2l+1} h(l,0)} \frac{\left\|2\pi\sqrt{\frac{4\pi}{2l+1}}h(l,0)\right\|^2}{\left\|2\pi\sqrt{\frac{4\pi}{2l+1}}h(l,0)\right\|^2 + A(l)} \end{aligned} \quad \text{E13}$$

where, $A(l)$ is ratio of angular power spectrum noise and angular power spectrum of signal($S_{NN}(l)/S_{FF}(l)$)

$$\begin{aligned} \hat{f}(l,m) = 2\pi\sqrt{\frac{4\pi}{2l+1}} k(l,0) s(l,m) = \\ \frac{1}{2\pi\sqrt{\frac{4\pi}{2l+1}}h(l,0)} \frac{\left\|2\pi\sqrt{\frac{4\pi}{2l+1}}h(l,0)\right\|^2}{\left\|2\pi\sqrt{\frac{4\pi}{2l+1}}h(l,0)\right\|^2 + A(l)} s(l,m) = \\ \frac{1}{r(l,m)} \frac{\|r(l,m)\|^2}{\|r(l,m)\|^2 + A(l)} s(l,m) \end{aligned} \quad \text{E14}$$

where, $r(l,m) = 2\pi\sqrt{\frac{4\pi}{2l+1}}h(l,0)$

Determination of Fiber Direction in High Angular Resolution Diffusion Images using Spherical Harmonics Functions and Wiener Filter

M. Hashemi Kamangar[a], M.R. Karami Mollaeia[a], R. Ghaderi[b]

[a] *Faculty of Electrical and Computer Engineering, Babol University of Technology, Babol, Iran*
[b] *Faculty of Control Engineering, Shahid Beheshti University, Tehran, Iran*

P A P E R I N F O

Paper history:
Received 12 May 2015
Received in revised form 28 February 2016
Accepted 03 March 2016

Keywords:
Diffusion Tensor MRI
High Angular Resolution Diffusion Imaging
Spherical Deconvolution
Wiener Filter
Orientation Distribution Function

چکیده

روش تصویربرداری دیفیوژن تانسور ام آر آی (DTI) یک روش تصویربرداری غیرمخرب از بافت‌های مغزی است، که در نواحی دارای فیبرهای متقاطع، مسیر فیبرها به درستی ارزیابی نمی‌گردند. به همین دلیل از تصاویر با قدرت تفکیک زاویه‌ای بالا (HARDI) برای ارزیابی مسیر فیبر در هر وکسل استفاده می‌گردد. یکی از روش‌های عمده برای مشخص نمودن راستای فیبرها در هر وکسل استفاده از دی‌کانولوشن کروی می‌باشد. دی‌کانولوشن کروی روشی است که به نویز بسیار حساس بوده و پیک‌های منفی در تابع توزیع جهت(ODF) فیبر ایجاد می‌کند. برای حل این مشکل از روش‌هایی از قبیل دی‌کانولوشن کروی لاپلاس–بلترامی(LB-SD)، دی‌کانولوشن کروی مبتنی بر گرادیان(GD-SD) و دی‌کانولوشن کروی مقید(CSD) استفاده می‌شود . در این مقاله، روشی برای دی‌کانولوشن کروی مبتنی بر فیلتر واینر (WB-SD) ارائه شده است. با توجه به نتایج، راستای فیبرهای متقاطع به درستی مشخص گردیده‌اند. الگوریتم پیشنهادی، راستای فیبرها را به ازای دو فیبر متقاطع با زاویه ۹۰ درجه به صورت صفر درجه با انحراف معیار ٤/٩ و ٨٩/٩ درجه با انحراف معیار ٣/٦ تشخیص داده است.

***doi**:10.5829/idosi.ije.2016.29.03c.07*